Fatigue Life Evaluation of Tripod Offshore Structure Using 3D Fatigue FE Analysis

Shazia Muzaffer[1] · Kyong-Ho Chang[1] · Wang-Sub Shin[1]

Abstract

Offshore wind power became an important source of renewable energy that is rapidly growing over the past several years. Large offshore wind turbines require strong and large support structures. The support substructures are exposed to diverse dynamic and static loads such as waves, snow, wind ice, earthquakes, and tides. These unstable, destructive repeated loads lead to material degradation or damage accumulation which in turn leads to the failure of offshore structures. Fatigue is considered one of the significant modes of failure in offshore structures. The constant exposure of welded multiplanar tubular joints of tripod structure under cyclic loading or the presence of flaws due to fabrication and construction induces high-stress concentration at these joints. The material degradation or damage accumulation at welded joints gives rise to the formation or propagation of cracks, and ultimately leads to a collapse of giant steel structures. This research aimed at investigating the origin of crack positions and fatigue life in tripod offshore structures. The 3-D fatigue FE analysis was carried out in two steps, Firstly, the welding deformation and welding residual stress were calculated in thermal and mechanical analysis. Secondly, 3D fatigue crack analysis based on cyclic hysteresis constitutive equation and fatigue damage theory was used to calculate the fatigue life and crack initiation in tripod offshores structure. Results obtained from the analysis were compared with the results from hot-spot stress method and Eurocode 3. From the results, it was considered that 3D-fatigue FEM is a useful method to estimate fatigue life and crack initiation.

Keywords Fatigue FEM · Fatigue crack initiation · Tripod · Offshore structures

List of symbols

A_n	Amplitude of octahedral shear stress
A_D	Damaged surface area
A_T	Total cross-section area of undamaged surface
C	Specific heat
D	Damage variable
D_N	Damage value at Nth cycle
D_d	Elastic–plastic material matrix
I	Arc current
K_X, K_Y, K_Z	Thermal conductivity
N	Number of cycles
N_f	Number of cycles to failure
Q(t)	Distributed heat flux
Q	Rate of moving heat generation per unit volume
Q_A	Heat input from the welding arc
Q_M	Energy induced by high-temperature melt droplets.
ro	Arc beam radius
U	Arc voltage
ɳ	Arc efficiency factor
ΔN	Increment of the number of cycles
b_i	Body force
σ_u	Ultimate stress
σ_{-1}	Fatigue limit of symmetrical loading
σ_r	Residual stress
σ_a	Stress amplitude
$\underline{\sigma}_{max}^{dev}$	Deviatoric tensor of maximum stress in the loading cycle
$\underline{\sigma}_{min}^{dev}$	Deviatoric tensor of minimum stress in the loading cycle
$\overline{\sigma}_H$	Hydrostatic stress
σ_{eq}	Equivalent of von Mises stress
σ_m	Mean stress

✉ Kyong-Ho Chang
changkor@cau.ac.kr

1   Department of Civil, Environmental and Plant Engineering, Chung-Ang University, 84, Hekseouk-ro, Dongjak-gu, Seoul 0697, Republic of Korea

σ_{max}	Maximum stress
$d\varepsilon$	Total strain increment
$d\varepsilon^e$	Elastic strain increment
$d\varepsilon^p$	Plastic strain increment
$d\varepsilon^{th}$	Thermal strain increment
dT	Temperature increment
σ_{ij}	Stress tensor
ρ	Density
D_d	Elastic–plastic material matrix

1 Introduction

Due to carbon neutrality and global warming, renewable power energy is nowadays booming. Renewable energy promises a future of clean or green energy by increasingly displacing traditional coal-fired or fossil-fired power. Renewables are nowadays becoming an essential power source while increasingly using more innovative and less expensive ways to capture solar, wind, and energy. The energy converter and wind turbine devices are used to capture these waves or wind motions and convert them into energy. The offshore wind turbines may be of fixed or floating type depending on the depth of water, type of loads, seabed soil properties, and cost of installation operations. The floating offshore wind turbines are constructed in areas where fixed offshore wind turbines are not feasible. Due to high expenses on installation, production, design, operation, application, and control of these floating offshore wind turbines, fixed offshore wind turbines are preferred better. The fixed offshore wind turbines during fabrication, installation, and operation in the harsh offshore environment, being subjected to different forces such as wind, earthquakes, waves, tides, and other offshore turbulences, due to which these offshore structures are susceptible to fatigue failure. Apart from this, the saline environment also adds damage through corrosion which widely existed in offshore support structures. The offshore support structures are designed to maintain safety during the in-service, reduction in prices as well as in space, have the adequate bearing capacity, and withstand different environmental conditions. Moreover, monitoring, inspection, maintenance, and repair had also been enforced to improve the service life of offshore wind turbine support structures. The tripod is the common type of fixed offshore substructure that is suitable in water depth of about 20–50 m (Kolios et al., 2010). The tripod is composed of a three-legged structure made from cylindrical tubes arranged in an equilateral triangle along with braces at the bottom part and a main monopile tubular section at the upper part. The heavy mass and the rotating turbine at the top transfers the load from the main monopile tubular section to the seabed through the tripod foundation. The fabrication of the three legs of tripod, braces, and a main monopile tubular section is by rolling and then welding relatively thick steel plates in longitudinal and circumferential directions. The constant exposure of these welded joints to an extremely harsh offshore environment leads to a continuous threat of material degradation due to metal corrosion and fatigue cracks due to the constant exertion of cyclic wave and wind forces. Fatigue is one of the most dominant failure modes in offshore structures which occurs when the structure is subjected to repeated loadings and results in the accumulation of plastic strain or damage. Therefore, accurate characterization of fatigue cracks in air and seawater environments can significantly provide accurate remaining fatigue life predictions, reduce maintenance efforts, improve efficient inspection plans, and reduce operational expenditure.

2 Literature Review

Moises Jimenez-Martinez (2020) discussed the fatigue damage caused by stochastic loadings, also the damage models used in the offshore analysis, and different types of offshores. The effect of asymmetrical and symmetrical configuration shape of fixed offshore structures on the buckling and fatigue analysis based on FEM was carried out by Muhammad Zubair Muis Alie (2016). Also carried out the nonlinear analysis of long-term fatigue due to Morison type forces as compared to a linearized approach for a drag-dominated offshore structure (Oleg et al., 2008). The effect of different conditions of scour under two-wave situations on the tripod foundation was examined for the fatigue limit state (FLS) the ultimate limit state (ULS) and, the serviceability limit state (SLS) (Hong Wang et al., 2008). Da Chen and Lijun Hou (2013) carried out the modal and coupled analysis of tripod structure using X-sea and FAST, found out that structural responses of tripod were far more superior than monopile substructure during static, modal and fatigue analysis. Also, under similar cyclic loading, the tripod structure has higher stiffness and longer fatigue life compared to the monopile structure. Joey Velarde and Erin Bachynski (2017) investigated that hydrodynamic load plays a dominant role in fatigue failure, its effect increases with the increase in water depth, so a fatigue damage parameter was determined to incorporate the fatigue damage effects caused by large wavefronts, wave peak period and significant wave heights. Yugang Li et al. (2014) carried out the refined fatigue analysis of tripod structure using ANSYS, presented the detailed modeling of local joint flexibility, a simplified approach to achieve an efficient reference for fatigue design of the support structure. Yeter et al. (2014, 2015, 2016) performed the joint spectral fatigue assessment of a tripod structure in the time domain or frequency domain under the combined cyclic wave and wind loading by using FEM and S–N fatigue damage approach. Peter Schaumann

et al. (2004) discussed the hybrid time–frequency domain fatigue analysis, an efficient method to demonstrate the damage prediction for deep-water tripod offshore platforms under wave loading. Hyawn Kim et al. (2018) analyzed the effects of load uncertainty on the fatigue life of wind turbine offshore structures. And the incorrect representation of load variation can lead to over-estimate or underestimate design lifetime, so it is important to consider the annual variability of sea load for accurate assessment of fatigue life of offshore support structures. Opaka et al. (2016) used the damage detection and localization method along with strain rosettes to determine the damaged structural member in offshore tripod structures. Wenbin Dong et al. () predicted the fatigue reliability of the welded multiplanar tubular joints of offshore structures considering the effect of corrosion. The geometry function effect and material degradation effect due to corrosion on the reliability analysis were determined. Jianhua Zhang et al. (2018) proposed a more cost-safety balanced design of a tripod offshore wind turbine, in which the design parameters are determined from combined reliability evaluation of the structure and statistical correlation analysis. Alati et al. (2014) studied the fatigue behavior of support structures under the combined stochastic wave and wind loading (Dolores et al., 2015).

This research is focused on predicting the high cycle fatigue life and crack initiation positions of tripod offshore support structures with weld joint using 3D fatigue FEM analysis. In this numerical analysis, the welding deformation and residual stresses are being calculated using 3D non-steady heat conduction FEM analysis and 3D thermal elastic–plastic FEM analysis. The fatigue life and crack initiation position are determined using a 3D nonlinear damage cumulative model formulated on continuum damage mechanics and cyclic hysteresis constitutive equation. The welding deformation and residual stresses are utilized as initial data of weld joints along with cyclic loading to calculate the fatigue life along with fatigue crack initiation and crack propagation directions. An interesting set of results from FE analysis were compared with the results of Structural Hot-Spot Stresses and Eurocode 3. The 3D fatigue FEM analysis method is useful to reduce the experimental costs and improve the structural integrity assessments of fatigue.

3 FE Welding Analysis Procedure

In today's modern world high attention is being paid to have innovative and less expensive materials. The materials with high yield strength, good ductility, ultimate tensile strength, and weldability are being considered to fulfill the ultra-high performance of huge structures. Welding is a complex, well-established process that involves the heating of metal parts until they are melted to join the different parts or materials. So, the individual members or joints of complex structures are connected by welding. The welded structures are subjected to multiple constant or variable loads ranging from cyclic, to completely random fluctuations. Thus, for the integrity of the whole structure, the resistance and load-carrying capacity of welded joints are of utmost importance for the safe operation of power plants, transmission pipelines, and offshore structures. Nevertheless, it must be remembered that different factors are affecting the resistance and load-carrying capacity of these welded structures like geometrical and metallurgical discontinuities, presence of flaws, environmental conditions, residual stresses, quality of the weld, and welding deformations. However, the welding residual stresses and deformations are inevitable, the presence of these undesirable stresses along with mechanical stresses significantly affect the fatigue behavior of welded structures. So, for accurate fatigue assessment, sound design, and safety of structure it is necessary to know about weld induced residual stresses and welding deformations. Many experimental techniques like the hole-drilling method, X-ray diffraction method, ultrasonic method, contour method, and neutron diffraction method could be utilized to measure the residual stresses but due to the complex geometries, time, and cost limitations numerical analysis has become a useful tool for analyzing the behavior of structures before construction. The numerical analysis is versatile, cost-saving, able to produce predictions that help in improving quality and productivity before carrying out the welding process. For the welding process with different complexities, many numerical modeling procedures have been recommended (Andres et al., 2011; Lindgren, 2006; Dean Deng et al., 2006, 2013; Yi et al., 2021; Chunbiao Wu et al., 2021; Park et al., 2021; Park et al., 2022). Using the in-house built FE code, the mechanism of welding was simulated using coupled 3-D thermo-mechanical formulations to capture the temperature histories, welding distortions, and phase transformations. To verify the validity of sequentially coupled 3-D thermo-mechanical formulations, experimental and numerical analysis results were compared, that are already published (Lee et al., 2007; Chang et al., 2006, 2011). In the thermal analysis, established on the constitutive heat conduction formulation, a non-linear temperature field is determined. The temperature histories collected in the previous step, are employed as thermal loadings, in the subsequent thermal elastoplastic analysis to find the structural response and capture the welding residual stresses, material, and geometric deformation.

3.1 FE Welding Analysis Model (DK-Type Joint)

Structures made of circular sections subjected to different loadings such as wind, water, and wave loading have proven to be the best shape. The offshore structures such as tripod

and jacket structures are mainly fabricated using circular hollow sections. The tubular joints used in jacket or tripod structures are usually fabricated by welding. These tubular joints are widely used due to their excellent mechanical properties, beautiful configuration, and high strength-weight ratio. This chapter aims to present FE modeling of a DK-type tubular joint of a tripod structure. The tripod is composed of a three-legged structure made from cylindrical tubes arranged in an equilateral triangle along with braces at the base part and a main monopile tubular section at the upper part as shown in Fig. 1. The rotating turbine at the top transfers the load from the main monopile tubular section to the seabed through the tripod foundation. Due to the complex shape, limitations of time, and symmetry of the joints at the base of the tripod, only one DK-type tubular joint needs to be modeled. The three braces connecting each other or to the main monopile tubular section are joined to the chord member by flux or core welding process. The brace and chord members were assumed to be joined by single-pass or instant welding. The fully penetrated butt weld between the members were created using flux-cored arc welding. The dimensions of DK-type tubular members are shown in Fig. 2. The weld region and immediate surrounding area during a welding process experience high temperature and dramatic stress gradients at different rates, so fine mesh is used to capture these structural responses. The fine mesh is provided at the weld region and in its surrounding area, while the mesh becomes coarser with the increase in distance from the weld centerline. The three-dimensional
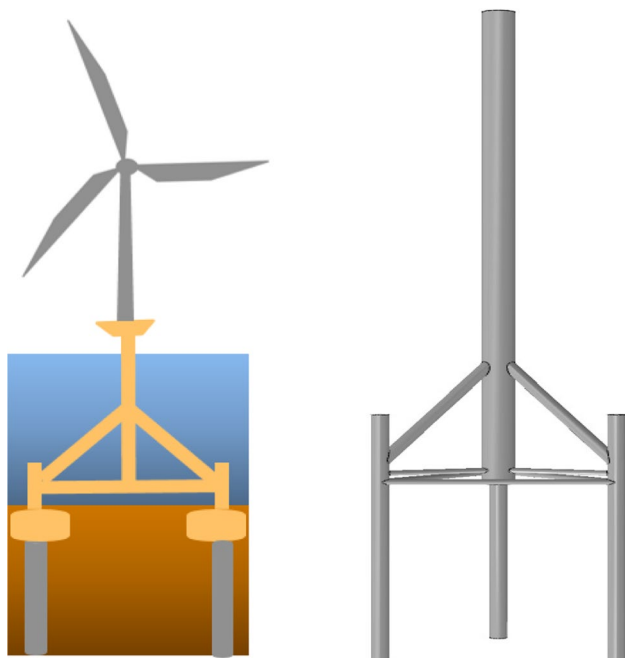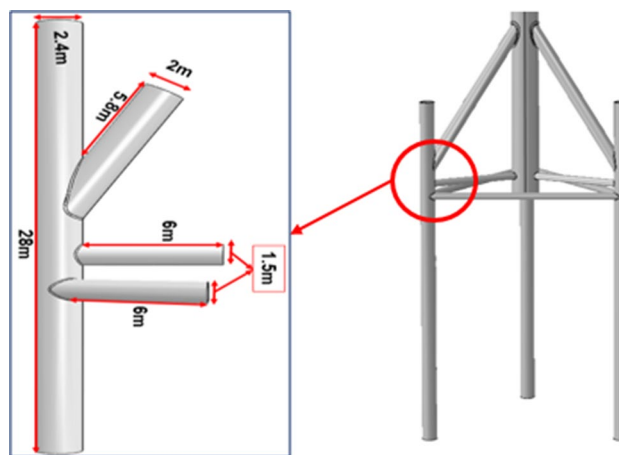

Fig. 2 Dimension of DK-type tubular joint

finite element mesh model, with eight-node isoparametric elements, is displayed in Figs. 3 and 4. To balance the calculation accuracy and computational time or data mapping between the two models i.e., thermal, and mechanical models, a similar mesh size was used, except for boundary conditions and element type. Each node of the element in the thermal model has one degree of freedom, temperature. Whereas each node of the element in the thermo-mechanical model has three translational degrees of freedom. Mesh sensitivity was investigated to examine the dependence of mesh size and mesh density on the veracity of results.

3.2 Welding Temperature and Thermal Elastoplastic Numerical Analysis

The thermal analysis solves for the phase evolution and temperature field as a function of time. The transient temperature and its distribution during welding are defined by the transient heat conduction equation, considering the temperature-dependent material characteristics.

$$\frac{d}{dx}\left(K_x\frac{\partial T}{\partial x}\right) + \frac{d}{dy}\left(K_y\frac{\partial T}{\partial y}\right) + \frac{d}{dz}\left(K_z\frac{\partial T}{\partial z}\right) + Q = \rho c\frac{\partial T}{\partial t}$$

(1)

The thermal model was used to reproduce the heat of the melt droplets and the welding arc. In the combined heat source model one part is the surface heat source (welding arc) with Gaussian distribution and the other part volumetric heat source (melt droplets) with uniform density. Within (r_0), at any time (t) the heat flux distribution on the surface of the workpiece is defined by the following equation.

$$Q(t) = \frac{3Q_A}{\pi r_0^2}\exp\left[-\left(\frac{r(t)}{r_0}\right)^2\right]$$

(2)

where,

Fig. 1 Tripod Structure

Fig. 3 The eight-noded isoparametric solid element

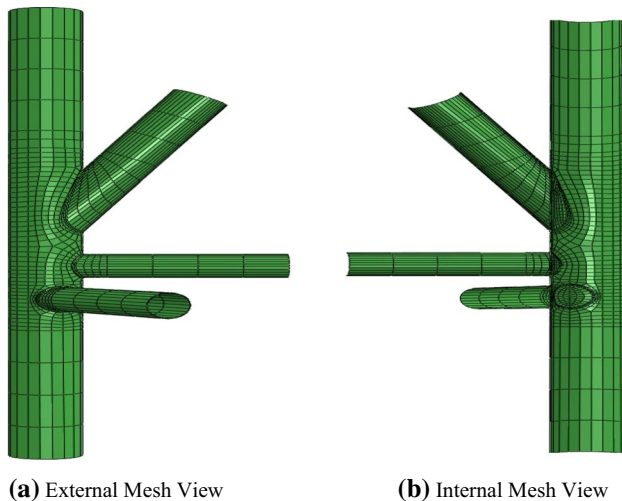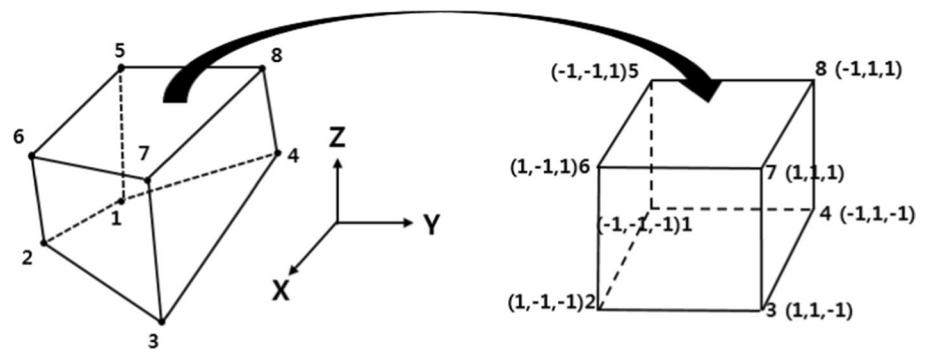**(a)** External Mesh View **(b)** Internal Mesh View

Fig. 4 Mesh view

$$Q_A = \eta \, I \, U - Q_M \tag{3}$$

The heat losses due to both radiation (dominant in and around the vicinity of the weld pool) and convection (dominant away weld pool) are taken into consideration by employing the total temperature-dependent heat transfer coefficient. The heat effects relevant to the fluid flow in the weld pool are considered by: (1) the thermal effects due to liquid–solid phase transformation of the weld pool are modeled by considering the latent heat for fusion, and (2) an artificial increase in the thermal conductivity was assumed for temperatures above the melting point. The solidus and liquidus temperatures and latent heat are 1450 °C, 1500 °C, and 270 J/g respectively.

In the subsequent thermo-mechanical analysis, the temperature histories i.e., thermal load computed in the thermal analysis are induced as input in the mechanical analysis. The accomplishment of mechanical analysis takes place using two sets of equations, the equilibrium equation, and the constitutive equation.

Equilibrium equation:

$$\sigma_{ij,j} + \rho b_i = 0 \tag{4}$$

The stress tensor is symmetrical, i.e., $\sigma_{ij} = \sigma_{ji}$.

Constitutive equation: The stress–strain relation in the incremental form is expressed as:

$$\{d\sigma\} = [D_d]\{d\varepsilon\} - \{c\}\mathrm{dT} \tag{5}$$

where $[D_d] = [D_d^e] + [D_d^p]$.

The insignificant effect of solid-state phase transformation (SSPT) on residual stresses during the welding process is considered, therefore the differential form of overall strain can be additively disintegrated into three components as follows:

$$\{d\varepsilon\} = \{d\varepsilon^e\} + \{d\varepsilon^p\} + \{d\varepsilon^{th}\} \tag{6}$$

where $d\varepsilon$ is total strain increment. The $d\varepsilon^e$, elastic strain increment is computed using isotropic Hook's law, with temperature-dependent Poisson's ratio and young's modulus. The $d\varepsilon^p$, plastic strain increment is calculated by employing a rate-independent elastoplastic constitutive equation, with the von Mises yield criterion, temperature-dependent mechanical properties, and linear isotropic hardening rule. The full Newton–Raphson iterative scheme is employed to obtain a useful solution. Meanwhile modifies the material properties and reformulates the stiffness matrix at each iteration step. This FE analysis has verified the FE results by comparing them with experimental data to confirm the veracity of the results obtained from this FE analysis (Shin et al., 2021; Lee et al., 2007; Chang et al., 2006, 2011). The temperature distribution gap for the DK-type tubular joint is shown in Fig. 5. The temperature-dependent thermal-physical (density, thermal conductivity, and specific heat) and mechanical properties (Poisson's ratio, thermal coefficient expansion, and yield stresses) of the base and weld metal were employed in the FE simulation. Figure 6 shows the temperature-dependent thermo-physical constants and temperature-dependent thermo-mechanical properties. The welding residual stresses in X, Y, and Z directions are displayed in Fig. 7. From the results, the tensile residual stresses occurred at the weld and in the vicinity while compressive

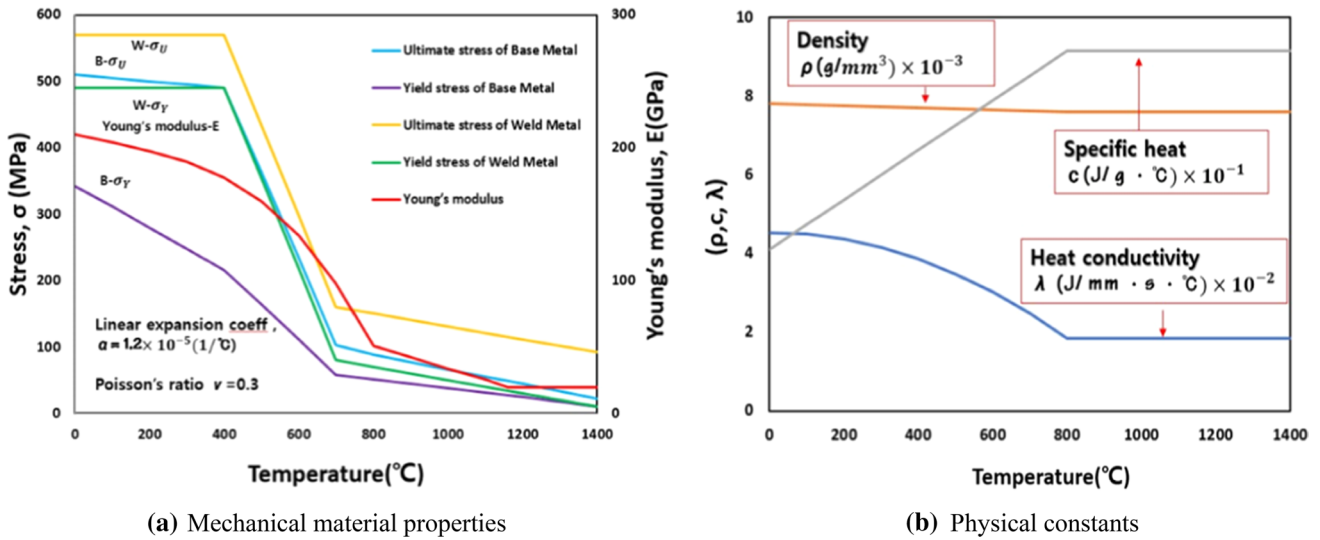(a) Mechanical material properties

(b) Physical constants

Fig. 5 Temperature-dependent physical constants and mechanical material properties
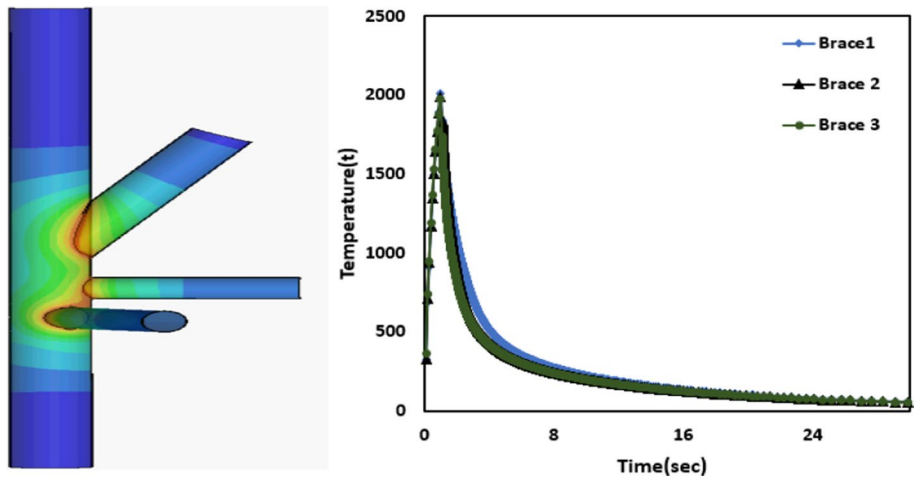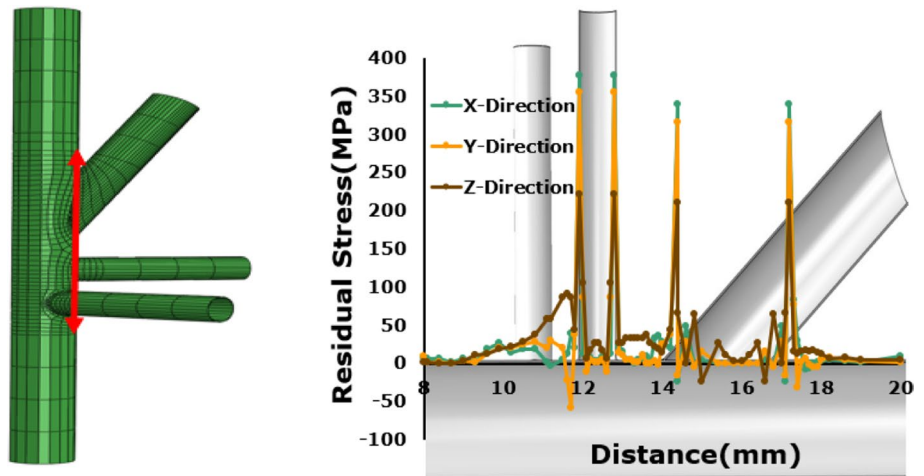
Fig. 6 Temperature distribution graph

Fig. 7 Residual stress distribution

residual stresses are found away from the weld. Also, it was found that the higher residual stresses were in X-axis (i.e., circumferential direction).

4 Fatigue FE Analysis for DK-Type Joint of Tripod Structure

A nonlinear damage cumulative model based on continuum damage mechanics combined with cyclic plasticity constitutive equations can be used to determine the total fatigue life of welded joints, with fatigue crack initiation and propagation. The fully coupled analysis method estimates the simultaneous solutions of fatigue damage evolution, stiffness degradation, and the cyclic derivation of constitutive equations including the microstructural changes (Chaboche et al., 1998; Abhinav et al., 2017; Lemaire, 1985; Pirondi et al., 2003; Zhang et al., 2012; Vuong et al., 2014, 2015a, 2015b; Lee et al., 2022). The nucleation of microcracks, growth, subsequent coalescence, and propagation under cyclic loading, affect the material behavior of the structure. So, this mechanical measurement of local damage, in the mechanics of continuous media is analyzed through homogenized variables in the representative volume element. For isotropic materials, the damage variable D representing the stiffness degradation defined by Kachanov (1958) and Lemaitre (1985) is given as

$$D = 1 - \frac{A_D}{A_T} \tag{7}$$

The concept of effective stress is induced by the damage variable (Kachanov, 1958), expressed as:

$$\overline{\sigma} = \frac{\sigma}{1 - D} \tag{8}$$

The coefficient (1-D) dividing the σ reduction factor, by which damage measurement can be achieved. At undamaged state the value of D = 0, at the partial damage state D = [0–1] whereas D = D_C indicates complete rupture, D_C is the critical damage value.

Under the multiaxial stress state, the 3D damage evolution model was proposed as:

$$\delta D = [1 - (1-D)^{\beta+1}]^{\alpha(\sigma_{Max}, \sigma_m)} \left[\frac{A_\Pi}{M(\sigma_m)(1-D)}\right]^\beta \delta N \tag{9}$$

with

$$\alpha(\sigma_{Max}, \sigma_m) = 1 - a\left(\frac{A_\Pi - A_\Pi^*}{\sigma_u - \sigma_{eq,max}}\right)$$

$$M(\sigma_m) = M_0(1 - 3b_2\overline{\sigma}_{H,mean})$$

where A_Π is the amplitude of the octahedral shear stress, defined in proportional loading as:

$$A_\Pi = \frac{1}{2}\sqrt{\frac{3}{2}\left(\underline{\sigma}_{max}^{dev} - \underline{\sigma}_{min}^{dev}\right) : \frac{3}{2}\left(\underline{\sigma}_{max}^{dev} - \underline{\sigma}_{min}^{dev}\right)}$$

The Sine criterion, with damage variable, is considered as:

$$A_\Pi^* = (1 - D)\sigma_{-1}(1 - 3b_1\overline{\sigma}_H)$$

An iterative method was used to repeat the analysis until the damage value was accumulated to reach the critical value, the crack initiation time of the structure. At that time the load-carrying capacity will be entirely lost, and the stiffness of the proportional element was rest to zero. The stress–strain and other state and associated variables are simultaneously updated for every cycle. The FE analysis was continuously going repeatedly until the crack propagated through the whole length of the weld. To conduct this type of analysis, the in-house FE code was used, extensively verified against the experimental and numerical data found in the literature (Vuong et al.,). The damage growth D, a function of the number of cycles N, and fatigue life N_f, can be estimated by integrating Eq. (9):

$$D = 1 - \left[1 - \left(\frac{N}{N_f}\right)^{1/(1-\alpha)}\right]^{1/(1+\beta)} \tag{10}$$

The number of cycles to failure is expressed as:

$$N_f = \frac{1}{(\beta+1)(1-\alpha)}\left(\frac{A_n}{M(\sigma_m)}\right)^{-\beta} \tag{11}$$

In an incremental form the damages are estimated as:

$$D_{N+\Delta N} = D_N + \Delta D \tag{12}$$

In multiaxial fatigue with the effects of welding residual stress, applied stress and the maximum stress under cyclic loading is distributed as:

$$\sigma_{max} = \sigma_a - \sigma_m \tag{13}$$

Considering the behavior of welding residual stress, the effective mean stress ($\overline{\sigma_m}$) is preferred in place of σ_m (mean stress)

$$\overline{\sigma_m} = \sigma_r + \sigma_m \tag{14}$$

The material and damage parameters determined from the experiment, Zhang et al. (2012) were needed to implement the FE analysis of high cycle fatigue under cyclic loading. The simulating of complex structures is a lengthy process

and takes a large amount of time and memory so, to eradicate these limitations jump-in cycle procedure was adopted. The method proceeds by evaluating the cyclic damage over one loading cycle followed by extrapolating the cyclic stress and accumulated plastic strain over the next block of cycles using Eqs. (8), (9) and (10). The repeated number of loading cycles before the termination of FE analysis was determined as fatigue life of the weld.
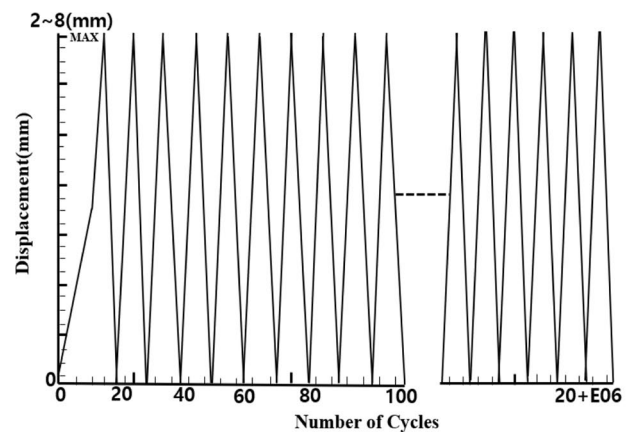
4.1 Boundary and Loading Condition of 3D Fatigue FEM Analysis

The welding residual stress, welding geometric, and material deformation obtained from thermo-mechanical analysis of the welding process were introduced as pre-stress (initial condition). The materials, geometry along mesh distribution were the same as used in the mechanical analysis, to make data mapping easier between two FE models. Eight-node isoparametric elements, with three translation degrees of freedom at each node, were considered. The cyclic fatigue loading was enforced as displacement control on the top of braces of DK-type joint with the lower limit of displacement as zero and maximum displacement applied was from 2 to 8 mm as denoted by red arrows in Fig. 8. The loads were applied to the transverse direction of the weld and during which the load ratio was kept zero. The nodes of loaded braces are kinematically coupled for translation in the corresponding direction to the applied load.

5 Results and Discussion

5.1 Comparison of Fatigue FEM Analysis and Structural Hot Spot Stresses with Eurocode 3

The fatigue results obtained from 3D fatigue FEM analysis were compared with the results of structural hotspot stress (HSS) and Eurocode 3 as shown in Fig. 12. The hot pot stress fatigue design approach has been designed for the fatigue assessment of offshore structures. The hot pot stress also called geometric stress, is the peak stress on the surface at the critical point where crack initiation is expected to occur. The hot spot stress is characterized as the maximum principal stress adjacent to the weld toe in the parent material, incorporating all the stress concentration effects due to overall geometry. As per IIW recommendations, the hot spot stresses are of two types, "a" and "b" type depending on the location and orientation of critical points in respect to weld toe as shown in Fig. 9. The hotspot stresses can be determined using extrapolation rules, which depend on the mesh size and position of hot spot points (located at the edge or on the surface). IIW recommends linear and quadratic

(a) Cyclic Load Type
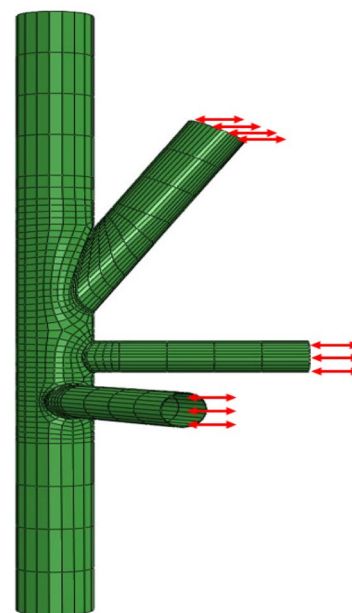
(b) Boundary and loading direction

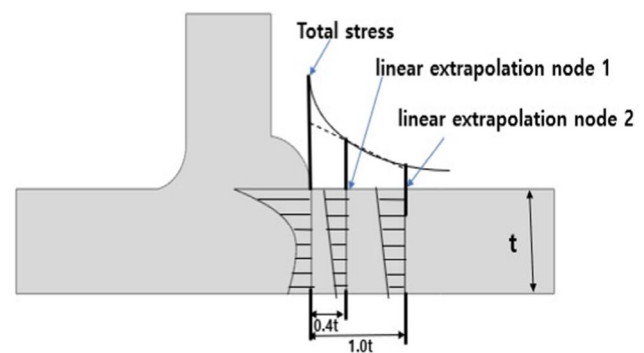**Fig. 8** Boundary and loading conditions

Fig. 9 Extrapolation method of hot spot stress

extrapolation rules, in this study linear extrapolation method, using fine mesh was employed to calculate the hot spot stress as shown in Fig. 10. The calculation formula designed to estimate the structural hot-spot stress is as.

$$\sigma_{hs} = 1.67\sigma_{0.4t} - 0.67\sigma_{1.0t} \qquad (15)$$

The extrapolation points are located at 0.4 t and 1.0 t from the weld toe as displayed in Fig. 11. The solid finite element model with reduced integration was adopted. The S–N curve is a logarithmic graph, that characterizes the relationship between cyclic stress and the number of cycles, with hot spot stress and equivalent stress range on the y-axis(ordinate) and the number of cycles on the x-axis(abscissa). Fatigue life assessments in the multiaxial state with complex loading and geometry result in multiple stress components. In this study to predict the fatigue life of DK- type joints in tri-pod structure under multiaxial cyclic loading, an equivalent stress range was used to transform the multiaxial stress state into the uniaxial stress state so that the material strength and fatigue life can be easily compared. The fatigue design S–N Curves of hot spot stress and FEM analysis were compared with S–N Curves recommended by Eurocode 3, the results were in good agreement with the S–N curves recommended by Eurocode 3. However, the results from hotspot stress were a little conservative and due to imitations, hot spot stress method was unable to detect the exact crack initiation positions as FE analysis (Fig. 12).

5.2 Crack Initiation Position in DK -Type Joint

In fully coupled elastic–plastic damage, internal stresses generated by external loading superpose with the residual stress, which in turn increases the mean stress effects as well as stress range. The damage rate is the function of mean
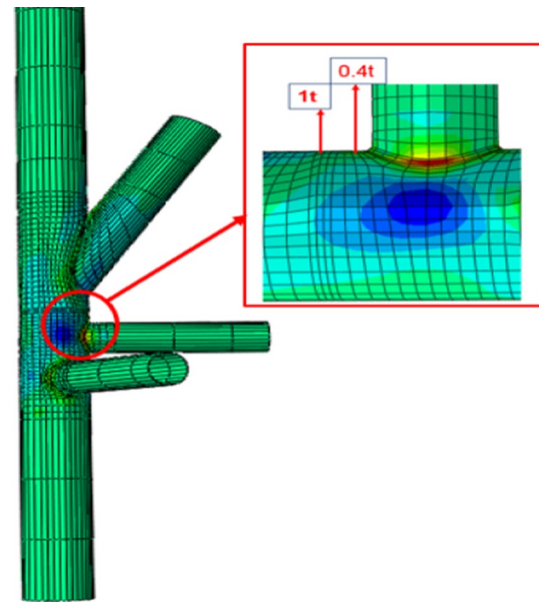

Fig. 11 Hot spot stress

stress that plays important role in reducing fatigue strength. Also, the residual stress significantly accelerates both the crack initiation and propagation. The crack in the damage model is defined as a total damaged area, with loss of stiffness and zero stress in the deformed area. The load-carrying capacity of the specimen gradually decreases with the crack initiation (Muzaffer et al., 2022; Kang et al., 2022; Wang et al., 2020). As the residual stresses were higher in the middle part, so crack initiation begins at the mid part of the DK-type joint and propagate around the entire joint as shown in Fig. 13. In real service structures it is difficult to exactly determine the crack initiation positions so, 3D
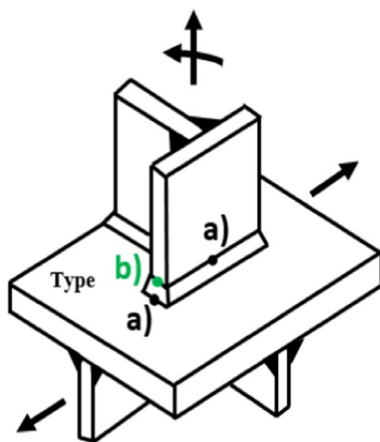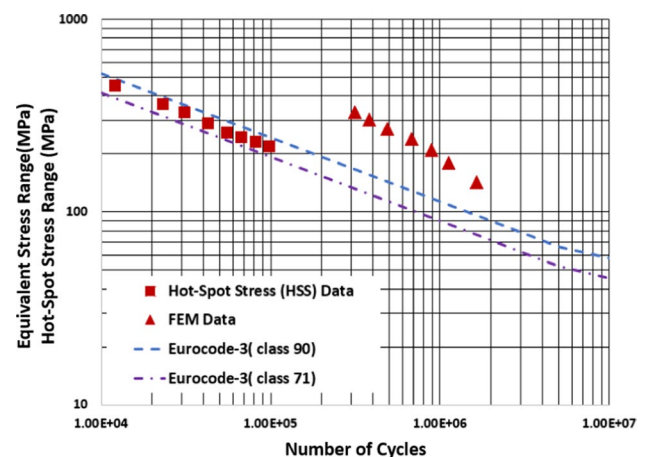

Fig. 10 Types of hot spots

Fig. 12 Comparison of results from fatigue FEA, HSS method with Eurocode 3
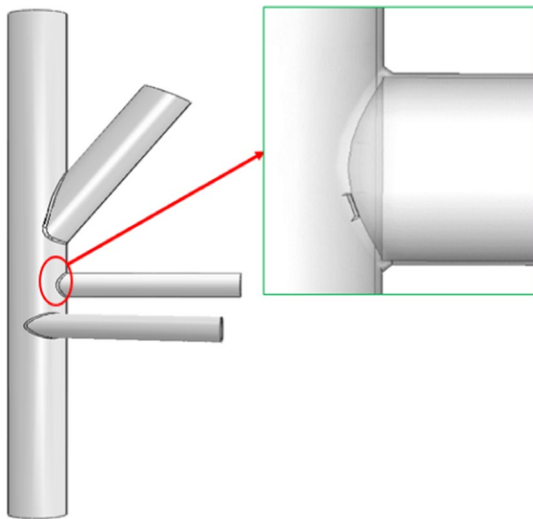
Fig. 13 Initial crack location

coupled damage-elastoplastic approach could give reasonable results corresponding to the behavior of real structures.

6 Conclusion

In this study, 3D thermal elastoplastic FEM analysis was conducted to evaluate the welding residual stresses and welding geometrical deformations. Subsequently, 3-D coupled damage-elastoplastic FE analysis was carried out, by utilizing welding residual stresses and welding geometrical deformation as the initial condition. The residual stress along with cyclic loading was considered as a parameter in the fatigue damage model to predict the fatigue life and crack initiation in the DK Type joint of the tripod structure. Although, there were many parameters such as load condition, thickness, diameter, weld type, and size, which affect fatigue performance of DK-type tubular members. In this study, welding residual stress and deformation were considered for fatigue analysis of DK-type tubular members subjected to cyclic loading. The following conclusions are drawn from the results.

1. The welding residual stress and deformation were considered for fatigue analysis.
2. The crack initiation and propagation direction were verified.
3. Under cyclic loading, the fatigue life of the DK-type tubular joint was predicted.
4. The fatigue FE analysis method is useful as a numerical tool for calculating the fatigue life.
5. The S–N curves from Hot Spots Stress, FE analysis were compared with S–N curves of Eurocode3, it was found

that FEA results were reliable as compared to Hot Spots Stress results.

Declarations

References

Alati, N., Nava, V., Failla, G., Arena, F., & Santini, A. (2014). On the fatigue behaviour of support structures for an offshore wind turbine. *Wind and Structures, 2014*(8), 117–134.

Anca, A., Cardona, A., Risso, J., & Fachinotti, V. D. (2011). Finite element modelling of the welding process. *Applied Mathematical Modelling, 35*, 688–707.

Chaboche, J. L., & Lesne, P. M. (1998). A non-linear continuous fatigue damage model. *Fatigue & Fracture of Engineering Materials & Structures, 11*, 1–17.

Chang, K. H., Kang, S. K., Wang, Z. M., Muzaffer, S., & Hirohata, M. (2019). Fatigue finite element analysis on the effect of welding joint type on fatigue life and crack location of a tubular member. *Archive of Applied Mechanics, 89*, 927–937.

Chang, K. H., & Lee, C. H. (2006). Characteristics of high-temperature tensile properties and residual stresses in weldments of high strength steels. *Materials Transactions, 47*, 348–354.

Chang, K. H., Lee, C. H., Park, K., & Um, T. H. (2011a). Experimental and numerical investigation on residual stresses in a multi-pass butt-welded high strength SM570-TMCP steel plate. *International Journal of Steel Structures, 11*, 315–324.

Chang, K. H., Lee, C. H., Park, K. T., & Um, T. H. (2011b). Experimental and numerical investigations on residual stresses in a multi-pass butt-welded high strength SM570-TMCP steel plate. *International Journal of Steel Structures, 11*, 315–324.

Chen, D., & Hou, L. (2013). Comparison of structural properties between monopile and tripod offshore wind-turbine support structures. *Advances in Mechanical Engineering, 5*, 175684.

Deng, D., & Murakawa, H. (2006). Numerical simulation of temperature field and residual stress in multi-pass welds in stainless steel pipe and comparison with experimental measurements. *Computational Material Science, 37*, 269–277.

Deng, D., & Murakawa, H. (2013). Numerical simulation of temperature and residual stress in multi-pass welds in stainless steel pipe and comparison with experimental measurements. *Thin-Walled Structures, 73*, 174–184.

Dolores Esteban, M., López-Gutiérrez, J. S., Negro, V., Matutano, C., García-Flores, F. M., & Millán, M. Á. (2015). Offshore wind foundation design: Some key Issues. *Journal of Energy Resources Technology, 137*, 051221–051231.

Kim, D. H., & Lee, G. N. (2018). Fatigue life evaluation of offshore wind turbine support structure considering load uncertainty. *The 2018 Structures Congress (Structures18),* Songdo Convesia, Incheon, Korea, August 27–31.

Dong, W., Moan, T., & Goa, Z. (2011). Long-term fatigue analysis of multi-planar tubular joints for a jacket-type offshore wind turbine in the time domain. *Engineering Structures, 33*, 2002–2014.

Dong, W., Moan, T., & Goa, Z. (2012). Fatigue reliability analysis of the jacket support structure for offshore wind turbine considering the effect of corrosion and inspection. *Reliability Engineering and System Safety, 106*, 11–27.

EN1993-1-1, Eurocode 3: Design of steel structures—Part 1–1: General rules and rules for buildings, 2005.

Gaidai, O., & Naess, A. (2008). Nonlinear effects on fatigue analysis for fixed offshore structures. *Journal of Offshore Mechanics and Arctic Engineering, 130*, 031009–031011.

Gautam, A., Ajit, K. P., & Sarkar, P. K. (2017). Fatigue damage estimation through continuum damage mechanics. *Procedia Engineering, 173*, 1567–1574.

Genry, M., Igoe, D., Dpherty, P., & Gavin, K. (2018). 3D FEM approach for laterally loaded monopile design. *Computer and Geotechnics, 100*, 76–83.

Kachanov, L. M. (1958). On the creep fracture time. *IzvAkadNauk USSROtd TEKH, 8*, 26–31.

Seong-Uk, K. (2020). Fatigue crack characteristics and prevention method in offshore steel tube jacket structures. Ph.D. Thesis.

Kang, S. K. (2022). Crack propagation characterization applying high manganese austenitic steel to independent type B tank. *Journal of Welding and Joining, 40*(1), 9–15.

Kolios, A., Collu, M., Chahardehi, A., Brennan, F. P., & Patel, M. H. (2010). A multi-criteria decision-making method to compare available support structures for offshore wind turbines. *EWEC, Europe's premier wind energy event,* Warsaw.

Lee, C. H., & Chang, K. H. (2007). Prediction of residual stresses in welds of similar and dissimilar steel weldment. *Journal of Materials Science, 42*, 6607–6613.

Lee, J. H., Kim, J. S., Kang, S. U., Hirohata, M., & Chang, K. H. (2017). Fatigue life analysis of steel tube member with T-shaped welded joint by FEM. *International Journal of Steel Structures, 17*(2), 833–841.

Lee, M. S., & Kim, M. H. (2022). Fatigue crack growth evaluation of IMO type B spherical LNG cargo tank considering the effect of stress ratio and load history. *Journal of Welding and Joining, 40*(1), 40–47.

Lemaitre, J. (1985). A continuous damage mechanics model for ductile fracture. *Journal of Engineering Materials and Technology, 107*, 83–89.

Li, Y., Chen, J., & Ren, N. (2014). Refined fatigue analysis for the tripod support structure of offshore wind turbine (OWT). *EJGE, 19*, 4193–4200.

Lindgren, L. E. (2006). Numerical modelling of welding. *Computer Methods in Applied Mechanics and Engineering, 195*, 6710–6736.

Ma, H., Yang, J., & Chen, L. (2018). Effect of scour on the structural response of an offshore wind turbine supported on tripod foundation. *Applied Ocean Research, 73*, 179–189.

Moises, J. M. (2020). Fatigue of offshore structures A review of statistical fatigue damage assessment for stochastic loadings. *International Journal of Fatigue, 132*, 105–327.

Muhammad Zubair, M. A. (2016). The effect of symmetrical and asymmetrical configuration shapes on buckling and fatigue strength analysis of fixed offshore platforms. *International Journal of Technology, 6*, 1107–1116.

Muzaffer, S., Chang, K. H., Wang, Z. M., & Kang, S. U. (2022). Comparison of stiffener effect on fatigue crack in KT-type pipe joint by FEA. *Welding in the World, 66*(4), 783–797.

Opoka, S., Soman, R., Mieloszyk, M., & Ostachowicz, W. (2016). Damage detection and localization method based on a frequency spectrum change in a called tripod model with strain rosettes. *Marine Structures, 49*, 163–179.

Park, S. Y., Kang, Y. J., Dongjin, O., Sangwoo, S., & Hong, H. U. (2021). Solidification cracking susceptibility of the weld metal of additively manufactured 316l stainless steel. *Journal of Welding and Joining, 39*(1), 45–50.

Park, T. U., Jung, D. H., Park, J. H., Kim, J. H., & Han, W. I. (2022). Changes in the mechanical properties and microstructure of high manganese steel by high heat input welding and general welding processes. *Journal of Welding and Joining, 40*(1), 33–39.

Pirondi, A., & Bonora, N. (2003). Modeling ductile damage under fully reversed cycling. *Computational Materials Science, 26*, 129–141.

Schaumann, P., & Kleineidam, P. (2004). Efficient fatigue design for tripod structures in north and baltic seas. In *DEWEK 2004-7th German wind energy conference*, Wilhelmshaven, 20th–21st October.

Shin, W., Chang, K. H., & Muzaffer, S. (2021b). Fatigue analysis of cruciform welded joint with weld penetration defects. *Engineering Failure Analysis, 120*, 105111.

Shin, W. S., Chang, K. H., & Shazia, M. (2021a). Fatigue analysis of cruciform welded joints with weld penetration defects. *Engineering Failure Analysis, 120*(2021), 105111.

Velarde, J., & Bachynski, E. E. (2017). Design and fatigue analysis of monopile foundations to support the DTU 10 MW offshore wind turbine. *Energy Preocdia, 137*, 3–13.

Vuong, N. V. D., Lee, C. H., & Chang, K. H. (2014). A nonlinear CDM model for ductile failure analysis of steel bridge columns under cyclic loading. *Computational Mechanics, 53*, 1209–1222.

Vuong, N. V. D., Lee, C. H., & Chang, K. H. (2015a). High cycle fatigue analysis in presence of residual stresses by using a continuum damage mechanics model. *International Journal of Fatigue, 70*, 51–62.

Vuong, N. V. D., Lee, C. H., & Chang, K. H. (2015b). A constitutive model for uniaxial/multiaxial ratcheting behavior of duplex stainless steel. *Materials and Design, 65*, 1161–1171.

Wang, Z. M., Chang, K. H., & Muzaffer, S. (2020). Fatigue analysis of the effects of incomplete penetration defects on fatigue crack initiation points in butt welded members. *Journal of Welding and Joining, 8*(6), 543–550.

Wu, C., Wang, C., & Kim, J. W. (2021). Welding distortion prediction for multi-seam welded pipe structures using equivalent thermal strain method. *Journal of Welding and Joining, 39*(4), 435–444.

Yeter, B., Garbatov, Y., & Guedes Soares, C. (2014). Spectral fatigue assessment of an offshore wind turbine structure under a wave and wind loading. In G. Soares & L. Peña (Eds.), *Development in maritime transportation and exploitation of sea resources.* Taylor & Francis Group.

Yeter, B., Garbatov, Y., & Guedes Soares, C. (2015). Fatigue damage assessment of fixed offshore wind turbine structures. *Engineering Structures, 101*, 518–528.

Yeter, B., Garbatov, Y., & Guedes Soares, C. (2016). Evaluation of fatigue damage model predictions for fixed offshore wind turbine support structures. *International Journal of Fatigue, 87*, 71–80.

Yi, M. S., & Seo, J. K. (2021). Residual stress study of high manganese steel riser pipe manufactured by longitudinal butt welding (1): residual stress measurement and FE analysis. *Journal of Welding and Joining, 39*(2), 135–143.

Zhang, J., Kang, W.-H., Zhang, C., & Sun, Ke. (2018). Reliability-based analysis and design of a tripod offshore wind turbine structure assuring serviceability performance. *Polish Maritime Research, 25*, 139–148.

Zhang, L., Liu, X. S., Wang, L. S., Wu, S. H., & Fang, H. Y. (2012). A model of continuum damage mechanics for high cycle fatigue of metallic materials. *Transactions of Nonferrous Metals Society of China, 22*(11), 2777–2782.